Ekman dynamics variability along the southern coast of Java revealed by satellite data

Anindya Wirasatriya , Joga Dharma Setiawan , Denny Nugroho Sugianto , Insan Alfi Rosyadi , Haryadi Haryadi , Gathot Winarso , Riza Yuliratno Setiawan & R. Dwi Susanto

Published online: 26 Aug 2020.

Submit your article to this journal ☑

View related articles ☑

View Crossmark data ☑

Taylor & Francis
Taylor & Francis Group

Check for updates

Ekman dynamics variability along the southern coast of Java revealed by satellite data

Anindya Wirasatriya [ID][a,b], Joga Dharma Setiawan[b,c], Denny Nugroho Sugianto [ID][a,b], Insan Alfi Rosyadi[a], Haryadi Haryadi[a], Gathot Winarso[d], Riza Yuliratno Setiawan [ID][e] and R. Dwi Susanto [ID][f,g]

[a]Department of Oceanography, Faculty of Fisheries and Marine Science, Diponegoro University, Semarang, Indonesia; [b]Center for Coastal Disaster Mitigation and Rehabilitation Studies, Diponegoro University, Semarang, Indonesia; [c]Department of Mechanical Engineering, Faculty of Engineering, Diponegoro University, Semarang, Indonesia; [d]Remote Sensing Application Center, National Institute of Aeronautics and Space of Indonesia, Jakarta, Indonesia; [e]Fisheries Department, Universitas Gadjah Mada, Jogjakarta, Indonesia; [f]Department of Atmospheric and Oceanic Science, University of Maryland, Maryland, USA; [g]Faculty of Earth Science and Technology, Bandung Institute of Technology, Bandung, Indonesia

ABSTRACT

It has been widely known that the coastal upwelling along the southern coast of Java is generated by southeasterly wind which induces offshore Ekman Mass Transport (EMT) during southeast monsoon. However, the variability of EMT has not been fully described in previous studies. The present study investigated the variability of Ekman dynamics which consist of EMT and Ekman Pumping Velocity (EPV) along the southern coast of Java, based on remotely sensed data. We demonstrated the incongruity between the distribution of southeasterly wind speed and sea surface temperature (SST) during southeast monsoon which is related to the distribution of Ekman dynamics. Offshore EMT at the western region of the southern coast of Java is stronger than offshore EMT at the eastern region. However, stronger offshore EMT at the western part is inhibited by downwelling EPV while weaker offshore EMT at the eastern part is accelerated by upwelling EPV. Consequently, SSTs at the eastern parts are lower than those at the western parts. Thus, the changes of offshore EMT intensity from eastern to western parts are balanced by their EPV distributions which explain the incongruity between the distribution of wind speed and SST during southeast monsoon. On an interannual time-scale, the combination of La Niña and negative Indian Ocean Dipole (IOD) events tends to weaken offshore EMT and EPV which reduce the intensity of Chl-*a* bloom and SST cooling during southeast monsoon season. Furthermore, ENSO has a less significant impact on the Ekman dynamics variability than IOD.

1. Introduction

Water mass lifting from the deeper water column to the sea surface is known as upwelling. This lifted water mass brings cold water which cools sea surface, and nutrient-rich water

CONTACT Anindya Wirasatriya ✉ aninosi@yahoo.co.id 📄 Department of Oceanography, Faculty of Fisheries and Marine Science, Diponegoro University, Jl. Prof. Soedarto, SH, Tembalang, Semarang, Indonesia, 50275

which is favourable for phytoplankton growth. Thus, lower sea surface temperature (SST) and higher sea surface chlorophyll-a (Chl-*a*) concentration are often used as indicators of an upwelling event. The increase of surface Chl-*a* concentration can escalate fisheries productivity (e.g. Sachoemar et al. 2010; Sachoemar, Yanagi, and Aliah 2012; Friedland et al. 2012; Racault et al. 2017; Zainuddin et al. 2017; Welliken et al. 2018). Thus, understanding upwelling characteristics in an area is fundamental for fisheries management.

The southern coast of Java (Figure 1) is known as a productive fishing ground for tuna (e.g. Syamsuddin et al. 2013, 2016; Lahlali et al. 2018). The production of bigeye tuna fishing, which is the most abundant tuna species in the southern coast of Java peaks during southeast monsoon season (Lahlali et al. 2018). This may be related to the upwelling event which also occurs during southeast monsoon season (e.g. Susanto, Gordon, and Zheng 2001; Susanto, Moore, and Marra 2006; Susanto and Marra 2005; Iskandar, Rao, and Tozuka 2009; Wirasatriya et al. 2018a). The southeasterly wind blowing along the southern coast of Java during southeast monsoon generates Ekman transport which pushes water mass away from the coast. The loss of water mass in the nearshore area is then replaced by the water mass from the deep water.

Based on the region classification of monsoon system based on the climatic rainfall in Indonesia by Aldrian and Susanto (2003), the southern coast of Java is located at region A which covers south and central Indonesia from south Sumatra to Timor Island, parts of Kalimantan, parts of Sulawesi, and parts of Papua. This region is characterized by strong seasonal variability of rainfall with strong influences of two monsoons, namely the wet northwest monsoon from November to March (NDJFM) and the dry southeast monsoon from May to September (MJJAS). The peak of northwest (southeast) monsoon occurs in December to February (June to August). Thus, March to May and September to November represent monsoon transitions. Along the southern coast of Java, the peak of southeast monsoon shifts to July, August, September, since the maximum speed of southeasterly wind occurs during this period (e.g. Susanto, Gordon, and Zheng 2001).

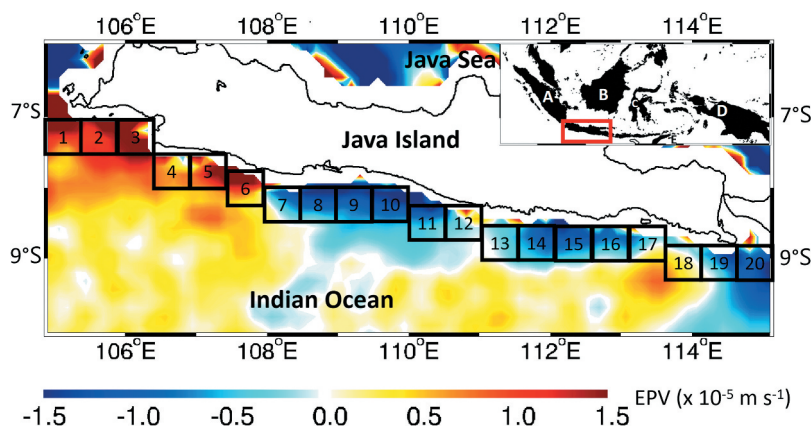**Figure 1.** Study area of southern coast of Java. Inset map is Indonesia. Background colour is Ekman Pumping Velocity (EPV) climatology in August. Positive (negative) EPV denotes downward (upward) water motion. Black boxes are distribution of 20 sample areas in 0.5° × 0.5° bins. A, B, C, D, and E in the inset map are Sumatra Island, Kalimantan Island, Sulawesi Island, Papua Island and Timor Island, respectively.

Some researchers proposed several factors that influence the upwelling generation along the southern coast of Java. For example, Kuswardani and Qiao (2014) stated that the blocking ITF could reduce coastal upwelling intensity along the southern coast of Java during the southeast monsoon season. ITF induces baroclinic instability that accelerates upwelling. By using Argo Float data, Horii, Ueki, and Ando (2018) found evidence of the upward movement of thermocline during southeast monsoon season due to upwelling which is concurrent with the anomalously southeasterly wind. Sea level drops are also identified in the tidal station data located along the western coast of Sumatra and southern coast of Java due to the upwelling occurs during southeast monsoon (Horii et al. 2016). Furthermore, Chen et al. (2016) explained that the shoaling thermocline signals which propagate into the southern coast of Java via equatorial Kelvin waves amplify the seasonal upwelling and cold SST anomalies during the summer-fall season (May to October). The influence of Kelvin wave is strong for interannual and intraseasonal variation of upwelling along the southern coast of Java (Chen et al. 2015, 2016; Delman et al. 2016, 2018; Horii, Ueki, and Ando 2018).

Among the factors mentioned above, wind speed is the most important factor that forms the seasonal pattern of coastal upwelling along the southern coast of Java Island (Susanto, Gordon, and Zheng 2001; Susanto and Marra 2005; Iskandar, Rao, and Tozuka 2009; Wirasatriya et al. 2018a). Nevertheless, the Ekman dynamics under the southeasterly wind that drive the upwelling generation were less described in the previous studies. It has been widely known that the generating mechanism of upwelling by the surface wind is through Ekman dynamics which consist of Ekman Mass Transport (EMT) and Ekman Pumping Velocity (EPV). Although Varella et al. (2016) showed the role of EMT on the variability of upwelling along the southern coast of Java, they neglected EPV in their analysis which may play important role in the upwelling processes. For example, in the Vietnamese coast, the different Ekman Dynamics trigger Chl-*a* blooming in a different season. During the southeast monsoon season, strong southerly wind constantly blowing in the eastern coast of Vietnam generating strong offshore EMT that causes coastal upwelling (Tang et al. 2004; Dippner et al. 2007). In contrast, chaotic wind occurs during intermonsoon season creating positive curl that generates upwelling EPV (i.e. negative EPV), then increases Chl-*a* concentration (Corrigan, Ramanathan, and Schauer 2006; Wang and Tang 2014). In the east coast of Peninsular Malaysia, EPV plays a more dominant role than EMT in generating upwelling during summer (Kok et al. 2017). In the California Current System, EPV is as important as EMT in generating upwelling (Pickett and Paduan 2003). In the present study, we demonstrate the contradict impact of EMT and EPV generated by southeasterly wind in driving the upwelling variabilities along the southern coast of Java. Furthermore, we also firstly show the seasonal and interannual variations of EMT and EPV along the southern coast of Java.

Because of the wide-ranging spatial coverage, and continues monitoring, remotely sensed data from satellite have often been used to investigate the ocean surface conditions within the Indonesian Seas (e.g. Susanto, Gordon, and Zheng 2001; Susanto and Marra 2005; Iskandar, Rao, and Tozuka 2009; Khaldun et al. 2018; Wirasatriya, Setiawan, and Subardjo 2017; Wirasatriya et al. 2018a, 2018b; 2019; Maisyarah et al. 2019; Bahiyah et al. 2019; Khasanah, Suprijanto, and Wirasatriya 2019; Suprijanto et al. 2019; Setiawan et al. 2019, 2020). Focusing the analysis on remote sensing data, the present study calculated Ekman dynamics from satellite-derived surface wind data for 12 years

observations (i.e. from 2007 to 2018) to investigate their spatial and temporal variability. Satellite-based data of SST and Chl-*a* are also used to investigate their impact on upwelling variability along the southern coast of Java.

2. Data and method

2.1. Data

For surface wind data, we used semi-daily Advanced Scatterometer (ASCAT) (Figa-Saldana et al. 2002) from 2007 to 2018. Spatial (longitude and latitude) resolutions of these datasets are 0.125° × 0.125°. This wind product is generated from a microwave scatterometer sensor which can estimate the speed and direction of the wind at about 10 m above the sea level. Moreover, this product has been tested and validated both for open seas and coastal areas and shows good accuracy for both areas (Verhoef and Stoffelen 2013).

SST and Chl-*a* data were obtained from daily Moderate Resolution Imaging Spectroradiometer (MODIS) Aqua Lv3 with the spatial resolution 0.04° × 0.04° (Esaias et al. 1998) from 2007 to 2018. Specifically, we chose MODIS SST obtained from11 μm since this product covers both day and night observation. MODIS Chl-*a* is only available in daytime observation since this product is built by using a visible band. Detailed explanation related to the algorithm for generating MODIS SST and Chl-*a* is described by Brown and Minnet (2009) and O'Reilly et al. (1998), respectively. Moreover, these datasets have been used and tested by many researchers (e.g.,Moore, Campbell, and Dowell 2009; Zhang et al. 2006; Ghanea et al. 2015; Lee et al. 2010; Qin et al. 2014).

We also used vertical profile data of temperature and salinity from GLOBAL-REANALYSIS-PHY-001-030 (Fernandez and Lellouche 2018), the ocean physics reanalysis distributed through the Copernicus Marine Environment Monitoring Service (CMEMS). This reanalysis data is generated by the NEMO platform with a grid interval of 0.083° × 0.083°. In addition, we also analysed the vertical profile data of temperature and salinity from Argo floats (Argo, 2000). We only chose the Argo floats which is located near the coastal line along the southern coast of Java.

2.2. Method

For calculating EMT and EPV, first, we converted surface wind data into wind stress (τ) by using the following equation:

$$\tau = \rho_a C_d U^2{}_{10} \tag{1}$$

where ρ_a is the density of air (1.25 kg m^{-3}), and U_{10} is the wind speed 10 m above sea level. The value of drag coefficient (C_d) follows WAMDI (1988) i.e.

$$1000 C_d = 1.29 \ \textit{for } 0 \ m \ s^{-1} < U_{10} < 7.5 \ m \ s^{-1} \tag{2a}$$

$$1000 C_d = 0.8 + 0.0065 U_{10} \ \textit{for } 7.5 \ m \ s^{-1} < U_{10} < 50 \ m \ s^{-1} \tag{2b}$$

Next, EMT and EPV were obtained using the following equations (i.e. Wang and Tang 2014):

$$EPV = -\frac{curl}{\rho_w f} \tag{3}$$

$$EMT = -\frac{\tau}{\rho_w f} \tag{4}$$

$$curl = \frac{\partial \tau_y}{\partial x} - \frac{\partial \tau_x}{\partial y} \tag{5}$$

where ρ_w is the density of seawater (1,025 kg m^{-3}) and f is the Coriolis parameter (Stewart 2008). The units of EMT and EPV are m^2 s^{-1} and m s^{-1}, respectively.

The previous studies (e.g. Pickett and Paduan 2003; Castelao and Barth 2006; Kok et al. 2017) converted the unit of EPV into vertical transport in order to compare the water mass transport brought by EMT and EPV in the same units (i.e. m^2 s^{-1}). They estimated vertical transport by integrating vertical velocity out to the distance where the positive wind stress curl remains. Since the present study is not only considering the positive wind curl stress but also negative wind curl stress, we did not convert into vertical transport. Helpern (2002) simply compared EPV and EMT which is represented by alongshore wind stress to examine the variability of Ekman dynamics off Peru during 1997–1998 El Niño. In the present study, we performed linear Pearson correlation analysis of the monthly data from 2007 to 2018 to determine the dominant role of the Ekman dynamics that influence upwelling along the southern coast of Java. Furthermore, we computed a multiple correlation coefficient of SST as a dependent variable and EPV and meridional EMT as independent variables to see how if both Ekman dynamics combine to influence SST variability along the southern coast of Java. We also calculated seawater density at the normal atmospheric pressure from the profiles of temperature and salinity by using the UNESCO's (1981) formula. All geophysical parameters were composited into monthly and monthly climatology. Monthly climatology is monthly means of all years (from 2007 to 2018).

To investigate the interannual variability of Ekman Dynamics along the southern coast of Java which may be influenced by El Niño Southern Oscillation (ENSO) and Indian Ocean Dipole (IOD), we used Oceanic Niño Index (ONI) and Dipole Mode Index (DMI), respectively. ONI index was obtained from https://www.cpc.ncep.noaa.gov/data/indices/oni.ascii.txt. The ONI index is the SST anomalies in the Niño 3.4 region (5°N-5°S, 170°W-120°W) with the basis period of 1971–2000. Meanwhile, the weekly DMI index is provided by https://stateoftheocean.osmc.noaa.gov/sur/ind/dmi.php. DMI is determined by the anomaly value of the SST gradient between the western tropical Indian Ocean (10°S-10°N and 50°E-70°E) and the southeastern tropical Indian Ocean (10°S-0°N and 90°E-110°E) (Saji et al. 1999). The anomaly is calculated relative to a monthly climatological seasonal cycle based on the years 1982–2005. The monthly climatology is linearly interpolated to determine weekly anomalies. In the present study, weekly DMI was composited into monthly DMI and smoothed it with 3-month running mean filter to reduce its high-frequency signal. We used ±0.5°C (±0.25°C) as a threshold to determine the period of El Niño and La Niña (positive and negative IOD).

3. Result and discussion

3.1. Spatial distribution of surface wind and SST during southeast monsoon along the southern coast of Java

Qu et al. (2005) have already provided monthly climatology map of surface wind and SST within Indonesian Seas which indicates good correspondence between SST and surface wind distribution. Moreover, Iskandar, Rao, and Tozuka (2009) also demonstrated good correspondence between the distribution of monthly climatology maps of surface wind and Chl-*a* along the southern coast of Java. In this section, we provide the finer scale maps of surface wind and SST during the peak of upwelling season, i.e. in August to expose the more detail relationship between surface wind and SST along the southern coast of Java (Figure 2a) which is missed by the previous studies. Cold SST (less than 26.5°C) spreads
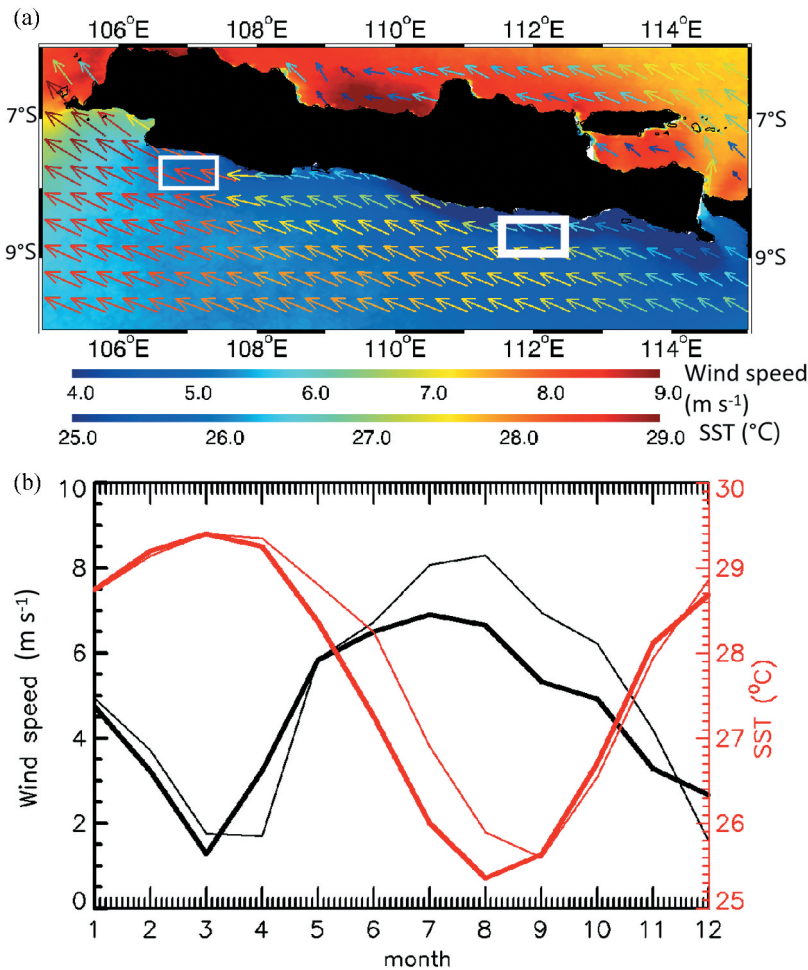

Figure 2. a) Distribution of monthly climatology data of SST and surface wind in August (2007–2018). Background colour is SST. Length of arrow and its colour denote wind speed. b) Monthly climatology of SST and wind speed. Thin and thick lines represent the mean values of SST and wind speed inside the thin and thick boxes in Fig. a.

unevenly along the southern coast of Java; cooler is the eastern region and warmer in the western region. Meanwhile, surface winds blow southeasterly along the southern coast of Java with speed by more than 6.5 m^{-1}. In contrast to the SST distribution, wind speed in the western region is higher than wind speed at the eastern region. Thus, there is an incongruity of the relation between surface wind speed and SST in the southern coast of Java where many studies in the different areas within the Indonesian Seas showed that the higher wind speed induced the cooler SST (Setiawan and Habibi 2011a; Setiawan and Kawamura 2011b; Setiawan et al. 2019, 2020; Wirasatriya, Setiawan, and Subardjo 2017; Wirasatriya et al. 2018b).

Furthermore, we extracted the mean values at two boxes in Figure 2(a) for SST and surface wind to test the relation between surface wind speed and SST at the western and eastern part of the southern coast of Java (Figure 2b). From January to March and from September to December, the variability of SST at the western and eastern boxes show a similar trend and value. Seasonal variation is robustly seen in both boxes. High SSTs occur twice a year in March and December which are maximum in March. Low SSTs also occur twice a year which are minimum in August for eastern box and September for the western box. This trend follows the variability of wind speed which also shows the seasonal variation. The wind speeds are minimum in March for both boxes and maximum in August and July for western box and eastern box, respectively. Focusing on the southeast monsoon/upwelling season (i.e. July to September), it can be seen that the wind speed at the western box is 1 m s^{-1} higher than the wind speed at the eastern box but in contrast, averaged SSTs in western box are higher by more than 0.5°C than averaged SSTs in eastern box. Thus, the inconsistency of the relation between wind speed and SST occurs during the upwelling season/southeast monsoon. To investigate this incongruity, we analysed Ekman dynamics as described in the next subsection.

3.2. Seasonal variation of Ekman dynamics

The seasonal variation of Ekman dynamics along the southern coast of Java is represented by EMT and EPV as shown in Figures 3 and 4, respectively. For EMT, onshore EMT is only observed in 4 months from December to March and attains a maximum in January denoted by the distribution of onshore EMT by about 4 m^2 s^{-1}. Onshore EMT occurs under the condition of northwesterly wind as has been shown by previous studies (e.g. Iskandar, Rao, and Tozuka 2009). On the other hand, offshore EMT dominates for all other seasons from April to November. Starting from April with the intensity of about 1 m^2 s^{-1}, offshore EMT attains a maximum in August denoted by the intensity by more than 2 m^2 s^{-1} along the southern coast of Java. Even more, in the western part, the offshore EMT is very strong (i.e. 8 m^2 s^{-1}). This condition follows the distribution of wind speed in August as shown in Figure 2(a). The weakest offshore EMT is observed in November before it changes into onshore EMT in December.

The seasonal variation of EPV along the southern coast of Java is also observed as shown in Figure 4. Positive and negative EPVs denote downward and upward velocities, which represent downwelling and upwelling processes, respectively. The weakest EPV occurs during the first transition season (March and April) denoted by nearly zero EPV ranges only from -0.5×10^{-5} m s^{-1} to 0.5×10^{-5} m s^{-1}. During the southeast monsoon (July, August, September) the amplitude of EPV is intensified ranges from -1.5×10^{-5} m s^{-1} to
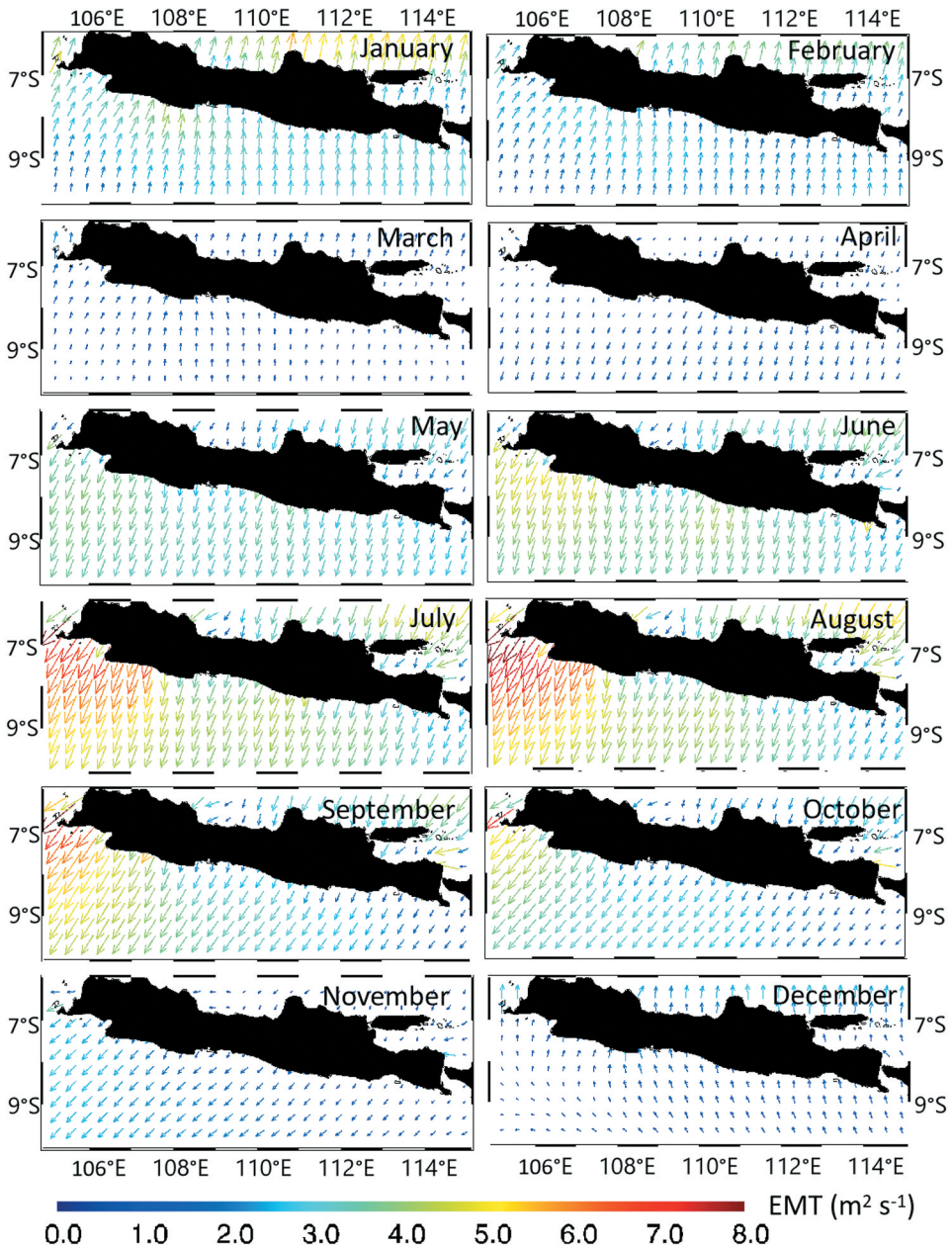
Figure 3. Monthly climatology of Ekman Mass Transport (EMT) from 2007 to 2018.

1.5×10^{-5} m s^{-1} along the southern coast of Java and peaks in August. Furthermore, we also can see the difference between EPV at the western part and eastern part of the southern coast of Java. At the western part, strong positive EPV indicates a strong downwelling process. In contrast, a strong upwelling process is identified at the eastern part of the southern coast of Java. The turning position between downwelling EPV and upwelling EPV along the southern coast of Java is located at 108.5°E.
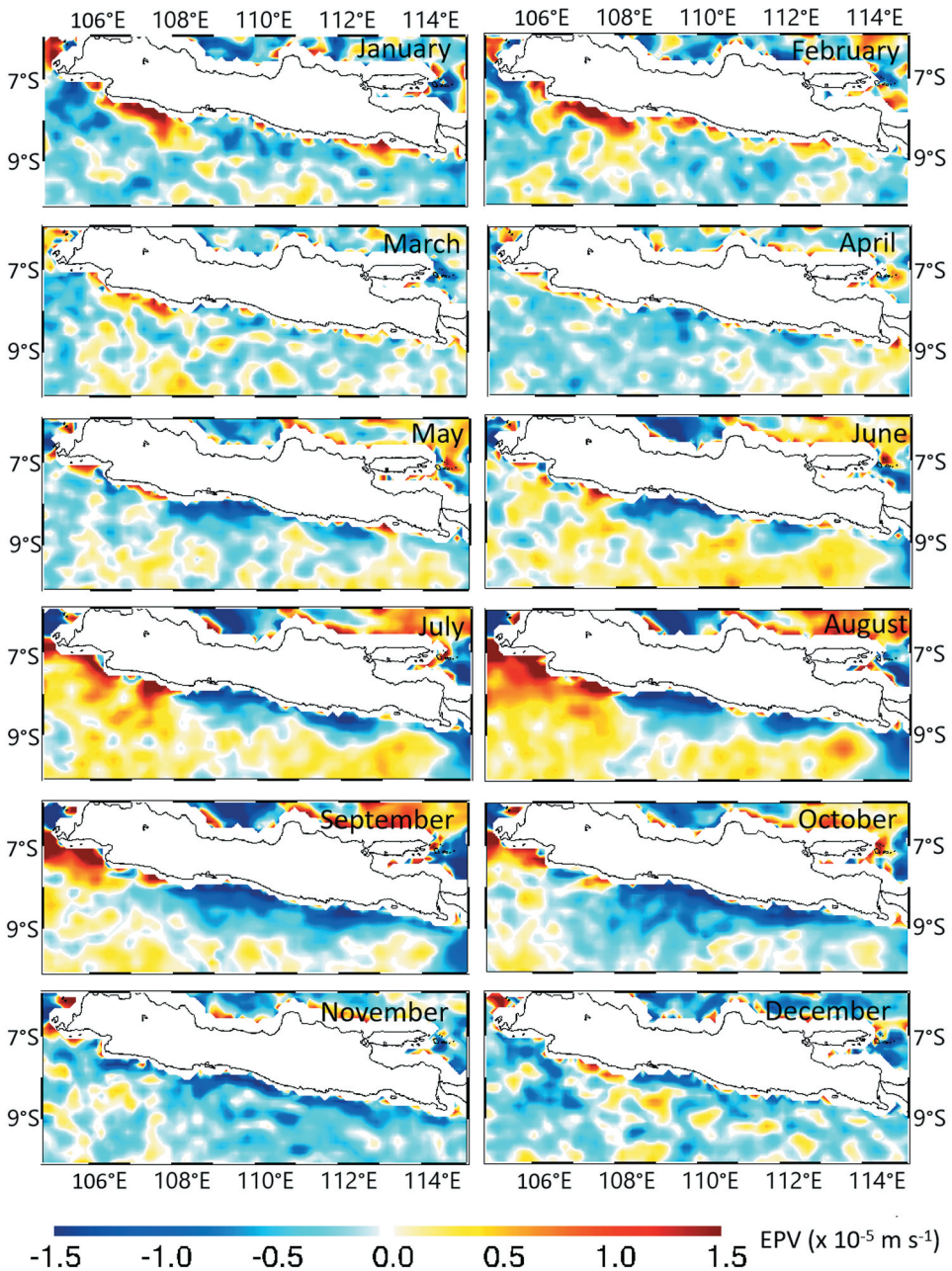
Figure 4. Monthly climatology of Ekman Pumping Velocity (EPV) from 2007 to 2018. Positive (negative) EPV denotes downward (upward) water motion.

To examine the relationship among EMT, EPV, and the distribution of SST, we averaged the meridional component of EMT and EPV in two boxes as shown in Figure 5(a). As described in the previous section, SST variations in both boxes are almost equal from January to March and from September to December. From April to August, SSTs in the eastern box is lower than the SSTs in the western box. From January to April, the
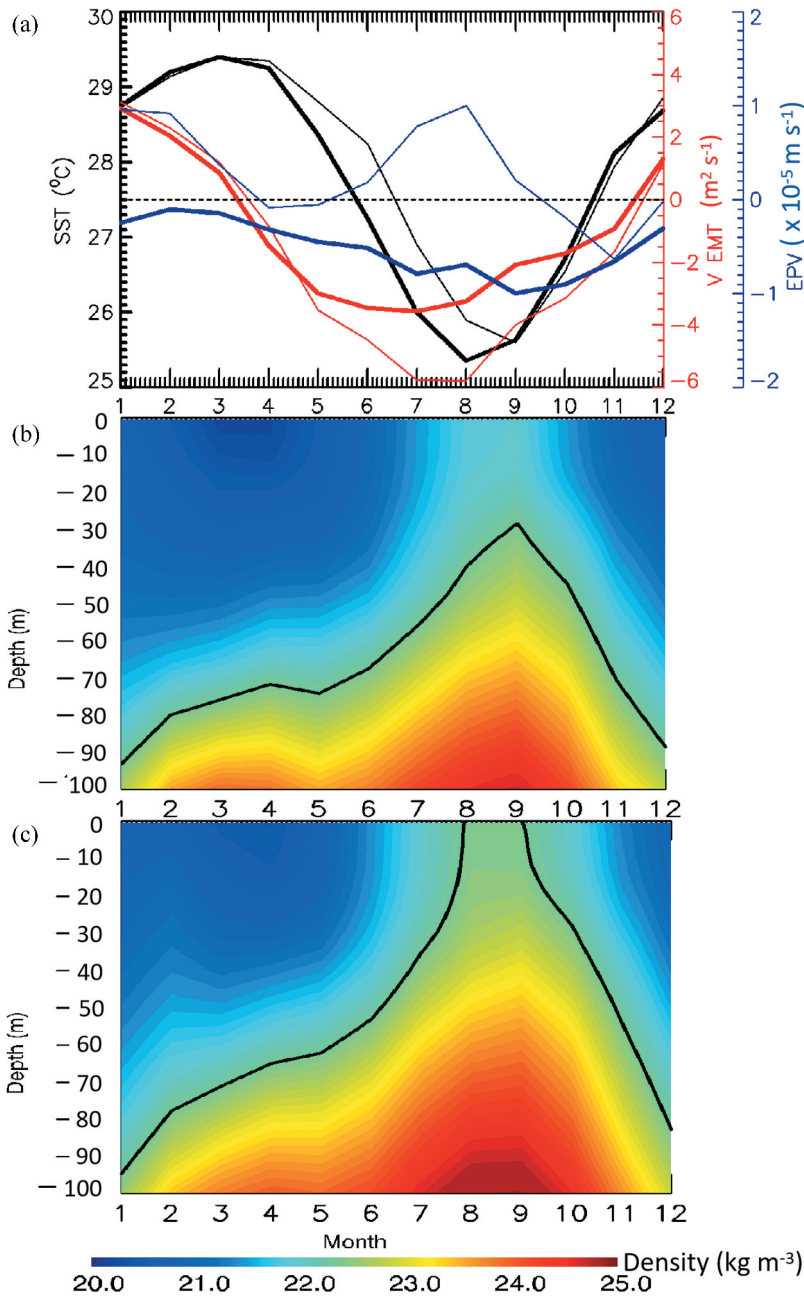
Figure 5. A) Monthly climatology of SST, meridional components of Ekman Mass Transport (EMT) and Ekman Pumping Velocity (EPV). Thin and thick lines represent the mean value inside the thin and thick boxes in Figure 2a. Positive (negative) EMT means onshore (offshore) EMT, respectively while positive (negative) EPV denotes downward (upward) water motion. b) and c) are monthly climatology of the vertical profile of sea water density at the normal atmospheric pressure inside the thin and thick boxes in Figure 2a, respectively. The black contours in b) and c) are isopycnals of 22.4 kg m^{-3}.

meridional component of EMTs in both boxes are also equal. After May, offshore EMT which is denoted by the negative meridional component of EMT in the western box becomes stronger than the eastern box. The difference of offshore EMT between two boxes attains a maximum in August. The difference of EPV between two boxes is also attained in August since during southeast monsoon season, EPV at the western boxes becomes positive, while at the eastern box, EPV is negative throughout the year. Thus, it can be concluded that during southeast monsoon, the eastern (western) box of the southern coast of Java is characterized by weak (strong) offshore EMT and negative (positive) EPV. This indicates that although coastal upwelling generated by offshore EMT at the eastern box is weak, negative EPV accelerates EMT generated upwelling. In contrast, the strong EMT generated upwelling at the western box is counteracted by the downwelling caused by positive EPV.

During northwest monsoon, onshore EMTs occur in both boxes. Furthermore, weak upwelling EPV occurs in the eastern box while downwelling EPV dominates in the western box. Thus, the decreased SSTs observed in January are not caused by Ekman dynamics. As reported by Chen et al. (2016), the SST anomaly during northwest monsoon is driven by surface heat flux. The high wind speeds may induce latent heat release which may cool SSTs in January for both boxes. As shown in Wirasatriya et al. (2019b), the variability of latent heat flux is induced by the wind speed that controls the variability of SSTs in the Java Sea.

The upwelling/downwelling processes in both boxes are represented by the variation of vertical density profiles obtained from reanalysis data as shown in Figure 5(b,c). The lifting of denser water masses which indicate upwelling occur during southeast monsoon season for both boxes. This observation is in accordance with a study of Chen et al. (2016) that revealed the shoaling of thermocline depth (depth of 23°C isotherm) off south Java during this season due to winds are upwelling favourable. However, it is clearly seen that the upwelling in the eastern box is stronger than in the western box as denoted by the higher surface density in the eastern box (i.e. more than 22.4 kg m^{-3}) from August to September. This result indicates that during the southeast monsoon season, weak off-shore EMT and negative EPV in the eastern box generate stronger upwelling than strong offshore EMT and positive EPV in the western box. As a result, SSTs in the eastern box are lower than those in the western box.

In accordance with the result from reanalysis data, the observation from Argo floats data also show the same tendency (Figure 6). The mixed layers depths during northwest monsoon season at the western and eastern area along the southern coast of Java are deeper than those during southeast monsoon season. Furthermore, it can be seen that during southeast monsoon season, the mixed layer depths at the eastern part are shallower than those at the western part. This indicates that the upwelling in the eastern part of the southern coast of Java is stronger than the western part.

Furthermore, we conducted a statistical analysis to obtain the relationship among SST, EMT, and EPV for both boxes as shown in Table 1. In the western box, the correlation between SST and meridional EMT is higher than the correlation between SST and EPV. This indicates that the influence of meridional EMT to SST variation is stronger than EPV. Conversely, the influence of EPV to SST variation is stronger than meridional EMT in the eastern box. However, the multiple correlation analysis between the meridional component of EMT and EPV as the independent variable and SST as the dependent variable is
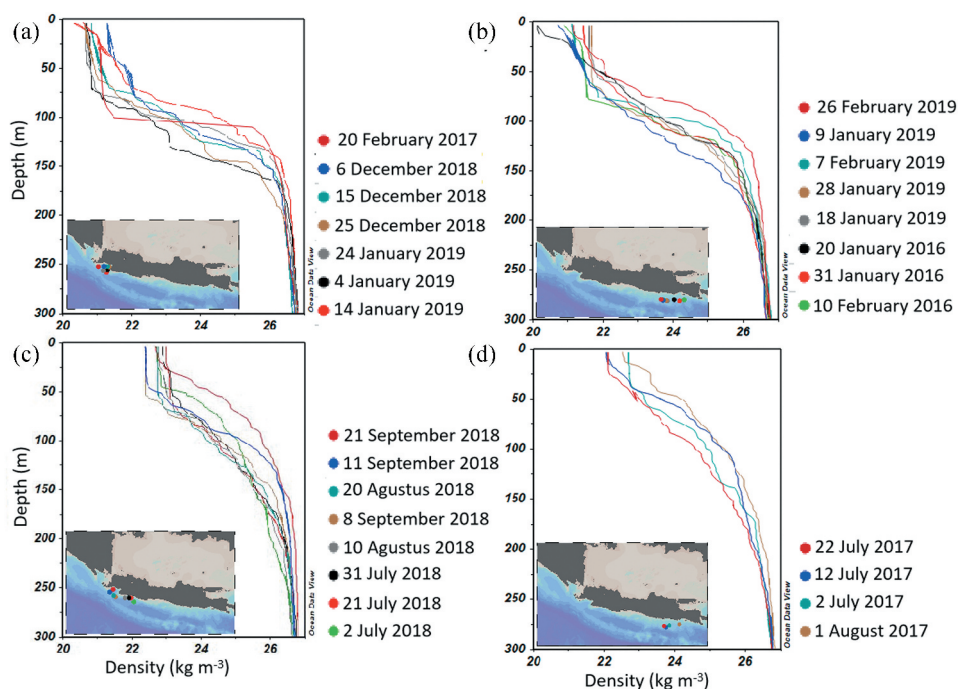
Figure 6. Vertical profile of density derived from Argo float data. Figure (a) and (b) denote northwest monsoon season while (c) and (d) denote southeast monsoon season.

Table 1. Highly significant correlation analysis ($p < 0.01$) among monthly SST, meridional EMT and EPV with range of time from 2007 to 2018 inside the thin (Western) and thick (Eastern) boxes as shown in Fig. 2a.

	Variable	EPV	Meridional EMT	EPV & Meridional EMT
SST	Thin Box (western)	0.34	0.53	0.63
	Thick Box (eastern)	0.55	0.49	0.64

stronger than the single correlation analysis for both boxes. The correlation coefficient in the western box is almost equal with the correlation coefficient in the eastern box. These correlation values imply that the effects of both wind speed (represented by EMT) and wind curl (represented by EPV) combine to influence SST variation along the southern coast of Java.

To investigate the zonal propagation of Ekman dynamics along the southern coast of Java, we took 20 sample areas in $0.5° \times 0.5°$ bins as shown in Figure 1. The bin size is determined by considering the range area of coastal upwelling which occurs only within the narrow band (about 70 km) along the coastal line (e.g. Horii, Ueki, and Ando 2018). We took monthly climatology averages for each bin and then plotted it in Hovmöller diagram (Figure 7). Westward propagation of offshore EMT is observed during southeast monsoon (from June to August). Westward propagation of downwelling EPV is also observed during southeast monsoon even though it slightly turns into negative in bin numbers 7 to 16. The westward propagation of Ekman dynamics also corresponds to
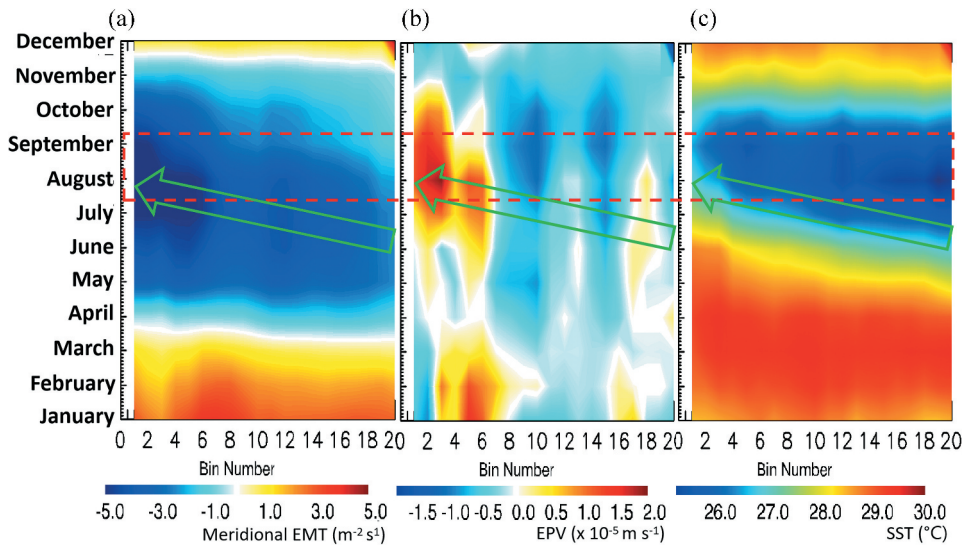
Figure 7. Hovmöller diagram of monthly climatology of meridional components of EMT, EPV and SST in the bins shown in Figure 1. Dashed red box denotes the peak of southeast monsoon in the months of August and September. Green arrows denote zonal propagation of meridional component of EMT, EPV and SST. Positive (negative) EPV indicates downward (upward) water motion, while positive (negative) EMT denotes onshore (offshore) EMT.

the westward propagation of low SST. The westward propagation of SST also has been presented in Susanto, Moore, and Marra (2006). A similar pattern of the zonal propagation of EMT also has been presented by Varella et al. (2016) in Figure 2 of their article. The westward propagation of offshore EMT corresponds to the westward propagation of low SST. Furthermore, they found that during the southeast monsoon season, the maximum offshore EMT occurs at 111°E. In our analysis, the position of 111°E is represented by box no. 12 which also shows the higher offshore EMT compared to its adjacent boxes during southeast monsoon season. Unfortunately, the westernmost analysis of Varella et al. (2016) was only until 109°E. Thus, the difference of offshore EMT between the western and eastern part as shown in the present study was missed in their analysis.

During the peak of the southeast monsoon season (dashed red box), offshore EMT is stronger at the western part than offshore EMT at the eastern part. At the western part (i.e. bin 1 to 6), offshore EMT reaches more than 5 m^2 s^{-1}. However, the western part of the southern coast of Java is dominated by strong downwelling EPV while upwelling EPV and low offshore EMT dominate at the eastern part. At the western part (i.e. bin 1 to 6), downwelling EPV reaches more than 0.5×10^{-5} m s^{-1}. As a result, the distribution of SSTs along the southern coast of Java is lower in the eastern part than the western part. This indicates that the inconsistency between wind speed and SST during southeast monsoon season along the southern coast of Java is related to the influence of wind curl which also plays an important role in generating upwelling/downwelling in the study area. At the areas where the southeasterly wind is strong, the wind curl tends to generate downwelling EPV that inhibits coastal upwelling induced by offshore EMT. In contrast, at the

areas with weak southeasterly winds, the wind curl raises strong upwelling EPV to accelerate the weak coastal upwelling that is generated by weak offshore EMT. As a result, upwelling in the western part is weaker than in the eastern part. Consequently, SST in the western part is higher than that in the eastern part.

Next, we plotted 12 years of monthly data of the meridional component of EMT and EPV in Hovmöller diagram (Figure 8a,b). Seasonal variation for the meridional component of EMT denoted by offshore and onshore EMT by turns during southeast and northwest monsoon season, respectively. Although the seasonal variation of EPV is not as robust as EMT, we still can see that during southeast monsoon season, the appearance of strong downwelling EPV at bin 1 to 6 may hamper the strong offshore EMT as mentioned in the previous subsection. At bin 7 to 20, enhanced upwelling EPV appears during the southeast monsoon season which can accelerate coastal upwelling caused by offshore EMT. Consequently, a high Chl-*a* band and low SST band are observed during southeast monsoon (Figure 9). In contrast, low Chl-*a* band and high SST band appear during northwest monsoon as a result of downwelling induced by onshore EMT and weak upwelling EPV.

3.3. *Interannual variation of Ekman dynamics*

To investigate the interannual variation of Ekman dynamics associated with ENSO and IOD, we compared the Hovmöller diagram of meridional component of EMT and EPV with the ONI and DMI indices (Figure 8c). Focusing on the southeast monsoon season, the most robust signals of interannual variation of Ekman dynamics are observed in 2010 and 2016, when offshore EMT and EPV are weakened. These cause the disappearance of the high Chl-*a* band and low SST band in 2010 and 2016 (Figure 9). These phenomena coincidence with La Niña and negative IOD events. A similar trend has also been found in other areas within the Indonesian Seas. For example, in the Lesser Sunda Islands which is located at the eastern side of the study area, weakened offshore EMT occurs when La Niña and Negative IOD events are in phase (Setiawan et al. 2019). Negative IOD and La Niña events also tend to increase SST and decrease Chl-*a* concentration in the Halmahera Sea due to the weakening southerly wind (Setiawan et al. 2020).

The interannual signals of EMT and EPV for the other years are not as robust as 2010 and 2016. However, we still can identify that during southeast monsoon season in 2007, 2008, 2011, 2012, 2015, 2017, and 2018, Chl-*a* (SST) is higher (lower) than the other years. During these events, strong offshore EMTs by lower than -5 m^2 s^{-1} are observed at the western parts (i.e. bin 1 to 6). In the eastern parts, enhanced upwelling EPV by lower than -1×10^{-5} m s^{-1} occur to strengthen upwelling. The periods of 2007 and 2011 are categorized as the in-phase of positive IOD and La Niña; 2008, 2012, 2017, and 2018 are positive IOD and normal ENSO; while 2015 is positive IOD and El Niño. This means that the effect of positive IOD is consistent to strengthen upwelling along the southern coast of Java regardless of the ENSO condition. In contrast, ENSO may have a less significant role to influence upwelling intensity along the southern coast of Java. This indication is supported by the statistical analysis which shows that the multiple correlation analysis between ONI (DMI) index and the combination of the meridional component of EMT and EPV during southeast monsoon (i.e. July, August, September) is 0.29 (0.51).
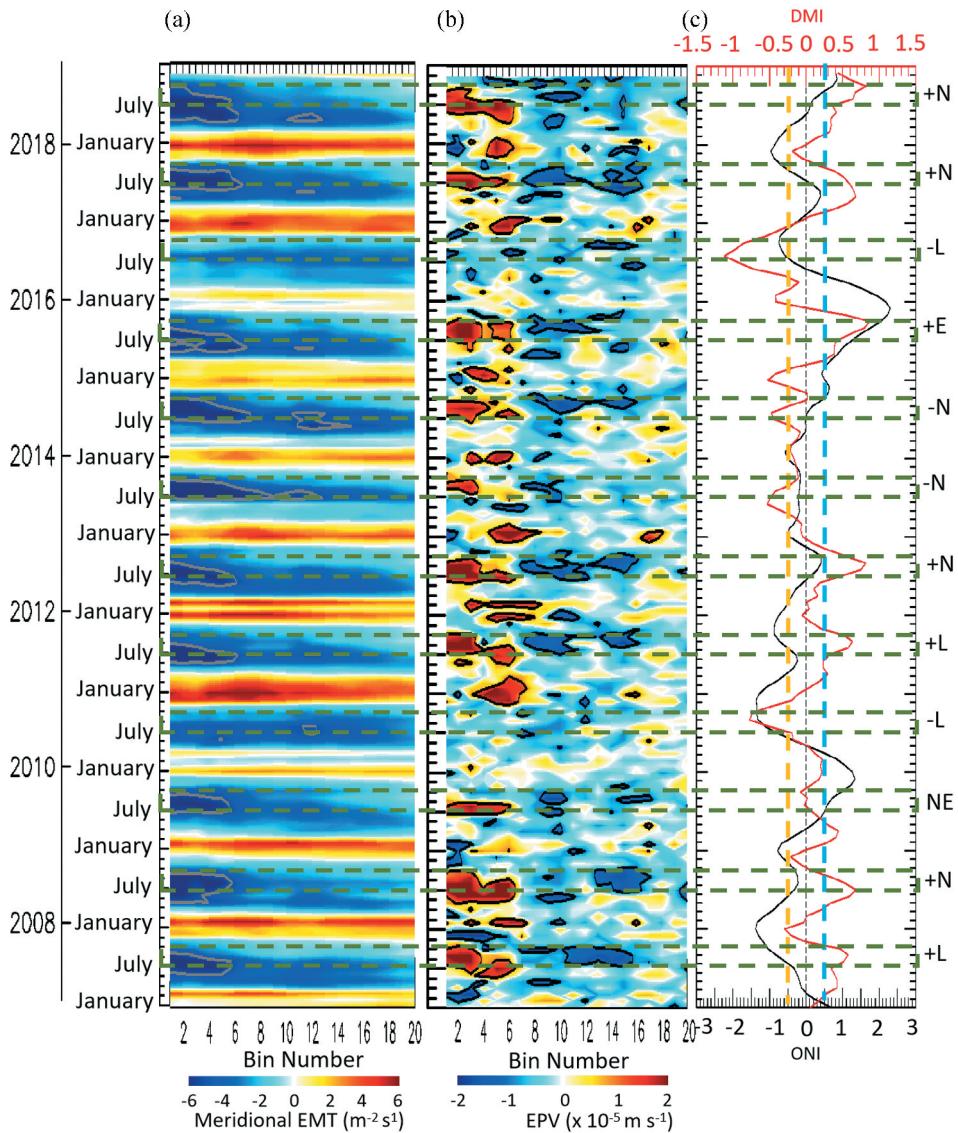
Figure 8. Hovmöller diagram of monthly data of meridional components of (a) meridional EMT, and (b) EPV in the bins showed in Figure 1. Gray contour in Fig. (a) denotes meridional EMT of -5 m^2 s^{-1}. Black contour in (Fig. b) denotes meridional of EPV $\pm 1 \times 10^{-5}$ m s^{-1}. Positive (negative) EPV indicates downward (upward) water motion, while positive (negative) EMT denotes onshore (offshore) EMT. (c) Time series of ONI (black) and DMI (red) indices. Dashed-green boxes indicate southeast monsoon season. The annotations on the right side of Fig. c indicate IOD and ENSO conditions i.e. '+' and '-' is for positive and negative IOD, respectively; 'E' and 'L' is for El Niño and La Niña, respectively; and 'N' is for normal IOD or ENSO. Blue dashed line indicates the threshold for positive IOD and El Niño, while yellow-dashed line is for negative IOD and La Niña.

This finding is consistent with Chen et al. (2016) which stated that IOD is more important than ENSO for amplifying upwelling off the southern coast of Java. Specifically, they suggest that the south Java upwelling events that occurred in 2003, 2006, 2007, 2008, and 2011 are more correlated to the DMI than the Niño-3 index. For the
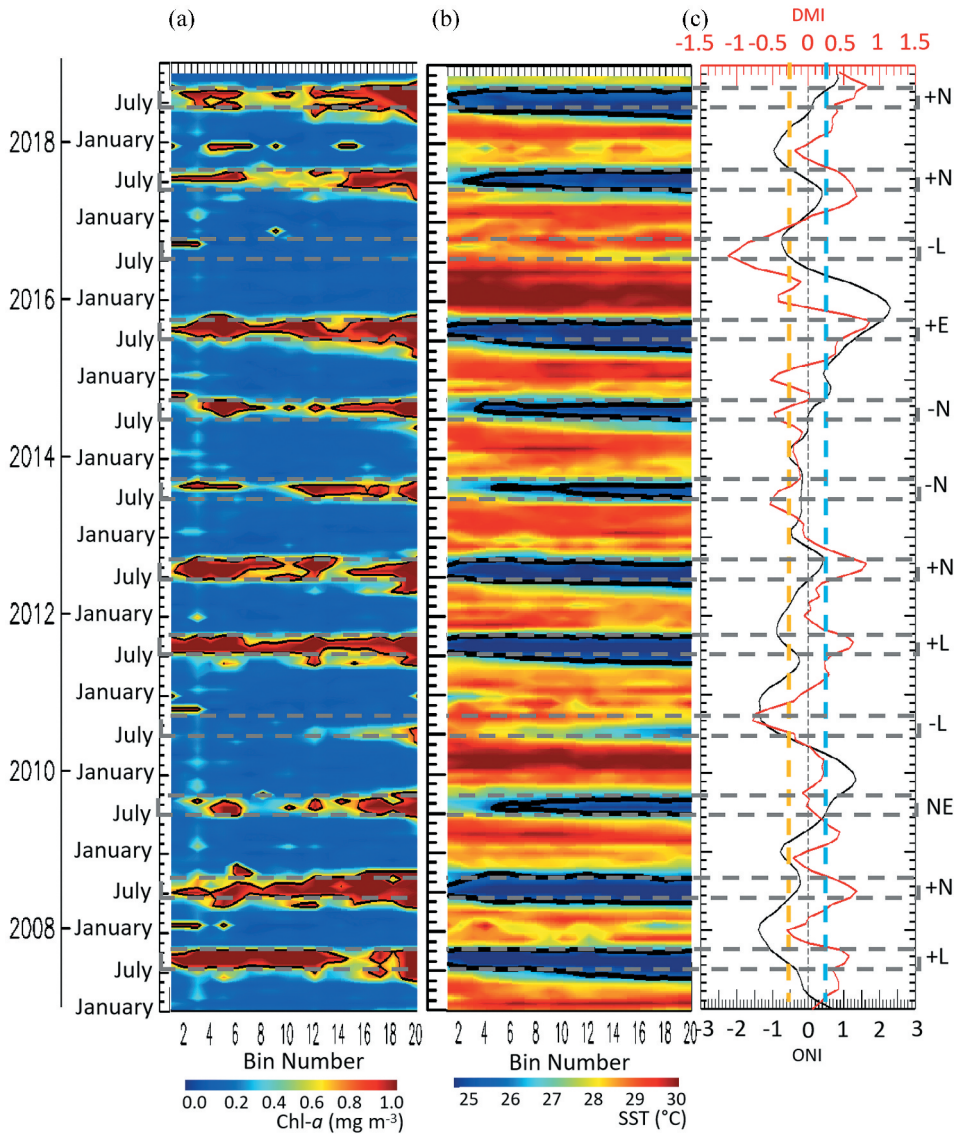
Figure 9. Hovmöller diagram of monthly data of (a) Chl-*a* and (b) SST in the bins showed in Fig. 1. Black contours in Fig. (a) and (b) denote Chl-*a* of 0.8 mg m^{-3} and SST of 26°C, respectively. (c) Time series of ONI (black) and DMI (red) indices. Dashed-green boxes indicate southeast monsoon season. The annotations on the right side of Fig. c indicate IOD and ENSO conditions i.e. '+' and '-' is for positive and negative IOD, respectively; 'E' and 'L' is for El Niño and La Niña, respectively; and 'N' is for normal IOD or ENSO. Blue dashed line indicates the threshold for positive IOD and El Niño, while yellow-dashed line is for negative IOD and La Niña.

El Niño events that took place in 2002 and 2009, there were no strong upwelling events observed in the south of Java. The equatorial Indian Ocean upwelling during southeast monsoon season associated with positive IOD is comparably influenced by local and remote forcings. Local forcing is related to the local wind stress, whereas in the present study is explained by EMT and EPV. Remote forcing is related to the propagation of Kelvin

waves along the equator and subsequently the western coast of Sumatra and the southern coast of Java driven by equatorial Indian Ocean winds (Chen et al. 2015, 2016; Delman et al. 2016, 2018; Horii, Ueki, and Ando 2018; Sprintall et al. 2000). Horii, Ueki, and Ando (2018) found the evidence for coastal Kelvin wave activity in July 2008, as Argo float data showed the upward movement of isotherms that was not supported by local wind anomalies. Furthermore, Delman et al. (2016) demonstrate the influence of Kelvin wave during strong positive IOD case in 2006. Alongshore wind anomalies near the coast of Java were neutral to slightly downwelling-favourable through much of the May–October upwelling season (e.g. Figure 8c, Delman et al. 2016). But there were upwelling-favourable winds along the equator and Sumatra coast in June 2006 as a precursor of Kelvin wave propagation, preceding the development of negative SST anomalies along the southern coast of Java.

Upwelling coastal Kelvin waves may affect surface chlorophyll as well. Like upwelling-favourable EMT and EPV from local wind forcing, Kelvin waves can bring deeper nutrient-rich waters close to the surface where they are entrained into the mixed layer (Chen et al. 2015). Some of this Kelvin wave variability (in particular equatorially generated Kelvin waves) are related to the IOD. Hence, strong positive Chl-*a* and negative SST anomalies can occur during the upwelling season when the DMI is positive, even when local EMT and EPV are not significantly different from their seasonal averages. Therefore, the high Chl-*a* and low SST during southeast monsoon season in 2007, 2008, 2011, 2012, 2015, 2017, and 2018 cannot be separated from the influence of the Kelvin wave-induced upwelling.

4. Conclusion

The variability of Ekman dynamics along the southern coast of Java and their relation to surface wind, SST and Chl-*a* have been investigated by using remote sensing data. The conclusions are as follows:

(1) There is an incongruity of the relation between the distribution of surface wind speed and SST in the southern coast of Java during southeast monsoon season. The higher the wind speed in the western areas is not followed by lower SST. This incongruity is related to the Ekman dynamics that influence the SST distribution along the southern coast of Java during the southeast monsoon.

(2) The seasonal variation of EMT along the southern coast of Java is dominated by offshore EMT which is favourable for generating coastal upwelling. Under the condition of southeasterly wind, offshore EMT occurs for 8 months from April to November and peaks in August. During southeast monsoon, offshore EMT at the western region of the southern coast of Java is stronger than offshore EMT at the eastern region.

(3) EPV during southeast monsoon season is stronger than EPV during the northwest monsoon season. During southeast monsoon season, positive (downward motion) EPV occurs at the western part of the southern coast of Java while negative (upward motion) EPV dominates at the eastern part.

(4) The increase in offshore EMT intensity from eastern to the western parts of the southern coast of Java during southeast monsoon are balanced by the changes of

EPV distribution which is negative in the eastern part and positive in the western part. As a result, upwelling in the eastern parts of the southern coast of Java is stronger than the western parts which result in lower SSTs in the eastern parts than the western parts.

(5) For interannual variation, the combination of La Niña and negative IOD events tend to weaken offshore EMT which reduces the intensity of Chl-*a* bloom and SST cooling during the southeast monsoon season. However, IOD plays a more significant role than ENSO to influence the variability of offshore EMT and EPV during southeast monsoon season since positive (negative) IOD consistently increases (reduces) the intensity of offshore EMT and EPV.

Disclosure statement

No potential conflict of interest was reported by the authors.

ORCID

Anindya Wirasatriya 🄳 http://orcid.org/0000-0003-1030-5126
Denny Nugroho Sugianto 🄳 http://orcid.org/0000-0002-1284-6471
Riza Yuliratno Setiawan 🄳 http://orcid.org/0000-0002-7987-9534
R. Dwi Susanto 🄳 http://orcid.org/0000-0003-1495-5951

References

Aldrian, E., and R. D. Susanto. 2003. "Identification of Three Dominant Rainfall Regions within Indonesia and Their Relationship to Sea Surface Temperature." *International Journal of Climatology* 23: 1435–1452. doi:10.1002/joc.950.

Argo. 2000. *Argo Float Data and Metadata from Global Data Assembly Centre (Argo GDAC)*. SEANOE. https://www.seanoe.org/data/00311/42182/

Bahiyah, A., A. Wirasatriya, J. Marwoto, G. Handoyo, and A. Anugrah. 2019. "Study of Seasonal Variation of Sea Surface Salinity in Java Sea and Its Surrounding Seas Using SMAP Satellite." *IOP Conference Series: Earth and Environment Science* 246 (2019): 012043.

Brown, O. B., and P. J. Minnett. 2009. "MODIS Infrared Sea Surface Temperature Algorithm Theoretical Basis Document", version 2.0 April, http://modis.gsfc.nasa.gov/data/atbd/atbd_mod25.pdf

Castelao, R. M., and J. A. Barth. 2006. "Upwelling around Cabo Frio, Brazil: The Importance of Wind Stress Curl." *Geophysical Research Letters* 33: L03602. doi:10.1029/2005GL025182.

Chen, G., W. Han, Y. Li, and D. Wang. 2016. "Interannual Variability of Equatorial Eastern Indian Ocean Upwelling: Local versus Remote Forcing." *Journal of Physical Oceanography* 46: 789–807. doi:10.1175/JPO-D-15-0117.1.

Chen, G., W. Han, Y. Li, D. Wang, and T. Shinoda. 2015. "Intraseasonal Variability of Upwelling in the Equatorial Eastern Indian Ocean." *Journal of Geophysical Research: Oceans* 120. doi:10.1002/2015JC011223.

Corrigan, C. E., V. Ramanathan, and J. J. Schauer. 2006. "Impact of Monsoon Transitions on the Physical and Optical Properties of Aerosols." *Journal of Geophysical Research* 111: D18208. doi:10.1029/2005JD006370.

Delman, A. S., J. Sprintall, J. L. McClean., and L. D. Talley. 2016. "Anomalous Java Cooling at the Initiation of Positive Indian Ocean Dipole Events." *Journal of Geophysical Research: Oceans* 121: 5805–5824. doi:10.1002/2016JC011635.

Delman, A. S., J. L. McClean, J. Sprintall, L. D. Talley, and F. O. Bryan. 2018. "Process specific Contributions to Anomalous Java Mixed Layer Cooling during Positive IOD Events." *Journal of Geophysical Research: Oceans* 123. doi:10.1029/2017JC013749.

Dippner, J. W., K. V. Nguyen, H. Hein, T. Ohde, and N. Loick. 2007. "Monsoon-induced Upwelling off the Vietnamese Coast." *Ocean Dynamics* 57 (1): 46–62. doi:10.1007/s10236-006-0091-0.

Esaias, W. E., M. R. Abbott, I. Barton, O. B. Brown, J. W. Campbell, K. L. Carder, D. K. Clark, et al. 1998. "An Overview of MODIS Capabilities for Ocean Science Observations." *IEEE Transactions on Geoscience and Remote Sensing* 36 (4): 1250–1265. doi:10.1109/36.701076.

Fernandez, E., and J. M. Lellouche. 2018. "Product User Manual for the Global Ocean Reanalysis Products GLOBAL-REANALYSIS-PHY-001-030". Marine Copernicus EU.

Figa-Saldaña, J., J. J. W. Wilson, E. Attema, R. V. Gelsthorpe, M. R. Drinkwater, and A. Stoffelen. 2002. "The Advanced Scatterometer (ASCAT) on the Meteorological Operational (Metop) Platform: A Follow on for European Wind Scatterometers." *Canadian Journal of Remote Sensing* 28 (3): 404–412. doi:10.5589/m02-035.

Friedland, K. D., C. Stock, K. F. Drinkwater, J. S. Link, R. T. Leaf, B. V. Shank, J. M. Rose, C. H. Pilskaln, and M. J. Fogarty. 2012. "Pathways between Primary Production and Fisheries Yields of Large Marine Ecosystems." *PLoS ONE* 7 (1): e28945.

Ghanea, M., M. Moradi, K. Kabiri, and A. Mehdinia. 2015. "Investigation and Validation of MODIS SST in the Northern Persian Gulf." *Advance Space Research* 57: 1. doi:10.1016/j.asr.2015.10.040.

Helpern, D. 2002. "Offshore Ekman Transport and Ekman Pumping off Peru during the 1997–1998 El Niño." *Geophysical Research Letters* 29 (5,1075): 1–4.

Horii, T., I. Ueki, F. Syamsudin, I. Sofiian, and K. Ando. 2016. "Intraseasonal Coastal Upwelling Signal along the Southern Coast of Java Observed Using Indonesian Tidal Station Data." *Journal of Geophysical Research: Oceans* 121: 2690–2708. doi:10.1002/2015JC010886.

Horii, T., I. Ueki, and K. Ando. 2018. "Coastal Upwelling Events along the Southern Coast of Java during the 2008 Positive Indian Ocean Dipole." *Journal of Oceanography* 74 (5): 499–508.

Iskandar, I., S. A. Rao, and T. Tozuka. 2009. "Chlorophyll-a Bloom along the Southern Coasts of Java and Sumatra during 2006." *International Journal of Remote Sensing* 30 (3): 663–671.

Khaldun, M. H. I., A. Wirasatriya, A. A. D. Suryo, and Kunarso. 2018. "The Influence of Indian Ocean Dipole (IOD) on the Variability of Sea Surface Temperature and Precipitation in Sumatera Island." *IOP Conference Series: Earth and Environment Science* 165 (2018): 012008.

Khasanah, U. N., J. Suprijanto, and A. Wirasatriya. 2019. "The Variability of Sea Surface Height Anomaly in the Seas along the Northern and Southern Coast of Java Island." *IOP Conference Series: Earth and Environment Science*. 246 (2019): 012049.

Kok, P. H., M. F. M. Mohd Akhir, F. Tangang, and M. L. Husain. 2017. "Spatiotemporal Trends in the Southwest Monsoon Wind-driven Upwelling in the Southwestern Part of the South China Sea." *PLoS ONE* 12 (2): e0171979.

Kuswardani, R. T. D., and F. Qiao. 2014. "Influence of the Indonesian Throughflow on the Upwelling off the East Coast of South Java." *Chinese Science Bulletin*. 59 (33): 4516–4523.

Lahlali, H., A. Wirasatriya, A. E. Gensac, M. Helmi, and R. A. Kismawardhani. 2018. "Environmental Aspects of Tuna Catches in the Indian Ocean, Southern Coast of Java, Based on Satellite Measurements." Paper presented at the 4th International Symposium on Geoinformatics 2018. Malang, Indonesia. 10-12 November. IEEE: 18380710. pp 1–6. DOI: 10.1109/ISYG.2018.8612020.

Lee, M. A., M. T. Tzeng, K. Hosoda, F. Sakaida, H. Kawamura, W. J. Shieh, Y. Yang, and Y. Chang. 2010. "Validation of JAXA/MODIS Sea Surface Temperature in Water around Taiwan Using the Terra and Aqua Satellites." *Terrestrial Atmospheric and Oceanic Sciences* 21 (4): 727–736. doi:10.3319/TAO.2009.09.07.01(Oc).

Maisyarah, S., A. Wirasatriya, J. Marwoto, P. Subardjo, and I. B. Prasetyawan. 2019. "The Effect of the ENSO on the Variability of SST and Chlorophyll-a in the South China Sea." *IOP Conference Series: Earth and Environment Science* 246 (2019): 012027.

Moore, T. S., J. W. Campbell, and M. D. Dowell. 2009. "A Class-based Approach to Characterizing and Mapping the Uncertainty of the MODIS Ocean Chlorophyll Product." *Remote Sensing Environment* 113: 2424–2430. doi:10.1016/j.rse.2009.07.016.

O'Reilly, J., S. Maritorena, B. G. Mitchell, D. Siegel, K. L. Carder, S. Garver, M. Kahru, and C. McClain. 1998. "Ocean Color Chlorophyll Algorithms for SeaWiFS." *Journal of Geophysical Research* 103: 24937–24953. doi:10.1029/98JC02160.

Pickett, M. H., and J. D. Paduan. 2003. "Ekman Transport and Pumping in the California Current Based on the U.S. Navy's High-resolution Atmospheric Model (COAMPS)." *Journal of Geophysical Research*. 108(C10):3327.

Qin, H., G. Chen, W. Wang, D. Wang, and L. Zeng. 2014. "Validation and Application of MODIS-derived SST in the South China Sea." *International Journal of Remote Sensing* 35 (11–12): 4315–4328. doi:10.1080/01431161.2014.916439.

Qu, T., Y. Du, J. Strachan, G. Meyers, and J. Slingo. 2005. "Temperature and Its Variability in the Indonesian Region." *Oceanography* 18(4):50–61. doi:10.5670/oceanog.2005.05.

Racault, M.-F., S. Sathyendranath, R. J. W. Brewin, D. E. Raitsos, T. Jackson, and T. Platt. 2017. "Impact of El Niño Variability on Oceanic Phytoplankton." *Frontier in Marine Science* 4: 1–15. doi:10.3389/fmars.2017.00133.

Sachoemar, S. I., T. Yanagi, N. Hendiarti, M. Sadly, and F. Meliani. 2010. "Seasonal Variability of Sea Surface Cholophyll-a and Abundance of Pelagic Fish in Lampung Bay, Southern Coastal Area of Sumatra, Indonesia." *Coastal Marine Science* 34 (1): 82–90.

Sachoemar, S. I., T. Yanagi, and S. R. Aliah. 2012. "Variability of Sea Surface Chlorophyll-a, Temperature and Fish Catch within Indonesian Region Revealed by Satellite Data." *Marine Research in Indonesia* 37 (2): 75–87. doi:10.14203/mri.v37i2.25.

Saji, N. H., B. N. Goswami, P. N. Vinayachandran, and T. Yamagata. 1999. "A Dipole Mode in the Tropical Indian Ocean." *Nature* 401: 360–363. doi:10.1038/43854.

Setiawan, R. Y., and A. Habibi. 2011a. "Satellite Detection of Summer Chlorophyll-a Bloom in the Gulf of Tomini." *IEEE Journal of Selected Topics in Applied Earth Observations and Remote Sensing* 4 (4): 944–948.

Setiawan, R. Y., A. Wirasatriya, U. Hernawan, S. Leung, and I. Iskandar. 2020. "Spatio-temporal Variability of Surface Chlorophyll-a in the Halmahera Sea and Its Relation to ENSO and the

Indian Ocean Dipole". *International Journal of Remote Sensing* 41 (1): 284–299. Advance online publication. doi:10.1080/01431161.2019.1641244.

Setiawan, R. Y., E. Setyobudi, A. Wirasatriya, A. S. Muttaqin, and L. Maslukah. 2019. "The Influence of Seasonal and Interannual Variability on Surface Chlorophyll-a off the Western Lesser Sunda Islands." *IEEE Journal of Selected Topics in Applied Earth Observations and Remote Sensing*. 12 (11): 4191–4197.

Setiawan, R. Y., and H. Kawamura. 2011b. "Summertime Phytoplankton Bloom in the South Sulawesi Sea." *IEEE Journal of Selected Topics in Applied Earth Observations and Remote Sensing* 4 (1): 241–244.

Sprintall, J., A.L. Gordon, R. Murtugudde, and R. D. Susanto. 2000. "A semi-annual Indian Ocean forced Kelvin waves observed in the Indonesian Seas, May 1997," Journal of Geophysical Research 105: 17217–17230. doi:10.1029/2000JC900065

Stewart, R. H. 2008. *Introduction to Physical Oceanography*. Texas A & M University, Texas, USA.

Suprijanto, J., I. Widowati, A. Wirasatriya, and U. N. Khasanah. 2019. "Spatio-Temporal Distribution of Chlorophyll-a in the Northern Waters of Central Java Using Aqua-MODIS." *IOP Conference Series: Earth and Environment Science* 246 (2019): 012050.

Susanto, R. D., A. L. Gordon, and Q. Zheng. 2001. "Upwelling along the Coasts of Java and Sumatra and Its Relation to ENSO." *Geophysical Research Letters* 28 (1): 1.559–1.602. doi:10.1029/2000GL011844.

Susanto, R. D., and J. Marra. 2005. "Effect of the 1997/98 El Nino on Chlorophyll-*a* Variability along the Southern Coasts of Java and Sumatra." *Oceanography* 4 (18): 124–127. doi:10.5670/oceanog.2005.13.

Susanto, R. D., T. Moore II, and J. Marra. 2006. "Oceanol. Color Variability in the Indonesian Seas during the SeaWiFS Era." *Geochemistry Geophysics Geosystems* 7 (5): 1–16.

Syamsuddin, M. L., S.-I. Saitoh, T. Hirawake, F. Syamsudin, and M. Zainuddin. 2016. "Interannual Variation of Bigeye Tuna (*Thunnus Obesus*) Hotspots in the Eastern Indian Ocean off Java." *International Journal of Remote Sensing* 37 (9): 2087–2100.

Syamsuddin, M. L., S.-I. Saitoh, T. Hirawake, S. Bachri, and A. B. Harto. 2013. "Effects of El Niño–Southern Oscillation Events on Catches of Bigeye Tuna (*Thunnus Obesus*) in the Eastern Indian Ocean off Java." *Fishery Bulletin* 111 (2): 175–188.

Tang, D. L., H. Kawamura, T. V. Dien, and M. A. Lee. 2004. "Offshore Phytoplankton Biomass Increase and Its Oceanographic Causes in the South China Sea." *Marine Ecological Progress Series*. 268: 31–41. doi:10.3354/meps268031.

UNESCO. 1981. "Tenth Report of the Joint Panel on Oceanographic Tables and Standards". UNESCO Technical Papers in Marine Science, Paris, 25

Varella, R., F. Santos, M. Gómez-Gesteira, I. Álvarez, X. Costoya, and J. M. Días. 2016. "Influence of Coastal Upwelling on SST Trends along the South Coast of Java." *PLoS ONE* 11 (9): e0162122.

Verhoef, A., and A. Stoffelen. 2013 "ASCAT Coastal Winds Validation Report", v1.5, May Technical Note SAF/OSI/CDOP/KNMI/TEC/RP/176, http://projects.knmi.nl/scatterometer/publications/pdf/ASCAT_validation_coa.pdf

WAMDI group. 1988. "The WAM Model: A Third Generation Ocean Wave Prediction Model." *Journal of Physical Oceanography* 1: 1775–1810. doi:10.1175/1520-0485(1988)018<1775:TWMTGO>2.0.CO;2.

Wang, -J.-J., and D. L. Tang. 2014. "Phytoplankton Patchiness during Spring Intermonsoon in Western Coast of South China Sea." *Deep Sea Res. II* 101: 120–128. doi:10.1016/j.dsr2.2013.09.020.

Welliken, M. A., E. H. P. Melmambessy, S. L. Merly, R. D. Pangaribuan, B. Lantang, J. Hutabarat, and A. Wirasatriya. 2018. "Variability Chlorophyll-a and Sea Surface Temperature as the Fishing Ground Basis of Mackerel Fish in the Arafura Sea." *E3S Web of Conferences* 73 (4004): 2018.

Wirasatriya, A., D. N. Sugianto, M. Helmi, L. Maslukah, R. T. Widiyandono, V. E. Herawati, P. Subardjo, et al. 2019b. "Heat Flux Aspects on the Seasonal Variability of Sea Surface Temperature in the Java Sea." *Ecology, Environment and Conservation*. 2 (1): 434–442.

Wirasatriya, A., D. N. Sugianto, M. Helmi, R. Y. Setiawan, and M. Koch. 2019a. "Distinct Characteristics of SST Variabilities in the Sulawesi Sea and the Northern Part of the Maluku Sea during the

Southeast Monsoon." *IEEE Journal of Selected Topics on Applied Earth Observations and Remote Sensing*. 12 (6): 1763–1770. doi:10.1109/JSTARS.2019.2913739.

Wirasatriya, A., I. B. Prasetyawan, C. D. Triyono, Muslim, and L. Maslukah. 2018b. "Effect of ENSO on the Variability of SST and Chlorophyll-a in Java Sea." *IOP Conference Series: Earth and Environment Science* 116(2018):012063.

Wirasatriya, A., K. L. Maslukah, A. Satriadi, and R. D. Armanto. 2018a. "Different Responses of Chlorophyll-a Concentration and Sea Surface Temperature (SST) on Southeasterly Wind Blowing in the Sunda Strait." *IOP Conference Series: Earth and Environment Science* 139 (2018): 012028.

Wirasatriya, A., R. Y. Setiawan, and P. Subardjo. 2017. "The Effect of ENSO on the Variability of Chlorophyll-a and Sea Surface Temperature in the Maluku Sea." *IEEE Journal of Selected Topics on Applied Earth Observations and Remote Sensing*. 10 (12): 5513–5518. doi:10.1109/JSTARS.2017.2745207.

Zainuddin, M., A. Farhum, S. Safruddin, M. B. Selamat, S. Sudirman, N. Nurdin, M. Syamsuddin, M. Ridwan, and S.-I. Saitoh. 2017. "Detection of Pelagic Habitat Hotspots for Skipjack Tuna in the Gulf of Bone-Flores Sea, Southwestern Coral Triangle Tuna, Indonesia." *PLoS ONE*. 12 (10): 1–19.

Zhang, C. Y., C. M. Hu, S. L. Shang, F. E. Muller-Karger, Y. Li, M. H. Dai, B. Q. Huang, X. R. Ning, and H. S. Hong. 2006. "Bridging between SeaWiFS and MODIS for Continuity of Chlorophyll-a Concentration Assessments off Southeastern China." *Remote Sensing Environment* 102: 250–263. doi:10.1016/j.rse.2006.02.015.